

The Effect of Hidden Radiant Ceiling Cooling Panel (RCCP) on Thermal Comfort and Energy Consumption in Ventilated Office Room with Transparent Ceiling: A CFD Analysis

Ahmed ElDegwy

Mechanical Power Engineering Department, Faculty of Engineering, Cairo University, Giza 12613, Egypt

E-mail address: mpdfoc_u_ahmed@cu.edu.eg

Abstract: The present study goal is to observe how the radiant ceiling performs in energy savings and thermal comfort in a ventilated office using CFD simulation. The boundary conditions for each CFD were all described. The profiles of air temperatures, Predicted Mean Vote (PMV), Predicted Percentage of Dissatisfied (PPD), and Draft Risk (DR) were examined to satisfy the comfort criteria of the ASHRAE standard. The effects of varying the temperature of the cooling panel, the air supply temperature, and the presence of air changes per hour (ACH) in the office space on thermal comfort and energy saving were investigated. A mesh is merged using more than 6 million optimized tetrahedral nodes. This investigation was reviewed to ensure that the program was consistent with the experimental results. The current study used the k- ϵ turbulence model after comparing it to previously published experimental results. Heat transmission by radiation was simulated using the Discrete Ordinates DO radiation model. This study found that the case selection (case 23252) actually has the advantage of energy-saving air conditioning, and its temperature is fixed at 25 °C, which is beneficial because the cooling water used in the cooling plate needs less energy than air in order to cool it (which has a large specific heat capacity and density). In this case, lower quality thermal systems such as geothermal energy or solar energy sources can be used to condition both the water and air supply.

Keywords: CFD; Radiant cooling; Energy saving; Thermal comfort; PMV

Symbol	Description	Symbol	Description
English letters			
a	Absorption coefficient	k_{eff}	Effective thermal conductivity [W/m.K]
B	Constant [0.261655 m ² .K/W]	n	Reflective index
C_{μ}	Coefficient of eddy-viscosity [-]	P	Local air pressure [Pa]
$C_{2\epsilon}, C_{3\epsilon}$	Constants	P_v	Water vapor pressure in humid air [Pa]
$D_{i,m}$	Mass diffusion coefficient of the i th species [m ² /s]	\vec{r}	Position vector
$D_{T,i}$	Soret diffusion coefficient [mole /m ² .s]	\vec{s}	Direction vector
E	Total energy [J]	S_i	Source term [mole /m ² .s]
H	Height [m]	S_k	Source term in kinetic energy equation [kg/m ³ .s]
\vec{g}	Gravitational acceleration [m/s ²]	S_{ϵ}	Source term in dissipation energy equation [kg/m ³ .s]

G_k	Production term of turbulent energy caused by average velocity gradient [kg/m ³ .s]	T	Air temperature [K]
G_b	The generation of turbulence kinetic energy due to buoyancy, [kg/m ³ .s]	T_a	inlet air supply temperature [K]
$G_{1\epsilon}$	Constant	T_{ma}	Average room temperature [K]
h	Enthalpy [J/kg]	T_{op}	Operation temperature [K]
h_c	Convective heat transfer [W/m ² .K]	T_p	Mean radiant ceiling temperature [K]
h_r	radiative heat transfer coefficient[W/m ² .K]	T_r	Average radiant temperature [K]
IT	Turbulence intensity [%]	\vec{v}	Velocity vector (m/s)
I	Radiation intensity	Y_i	Mass fraction [-]
\vec{J}_l	Diffusion flux [mole /m ² .s]	Y_M	The contribution of the fluctuating dilatation to the overall dissipation rate
k	Turbulent kinetic energy [J/kg]		
Greek symbols			
ρ	Density [kg/m ³]	μ_t	Eddy viscosity [Pa·s]
ϵ	Dissipation rate [m ² /s ³]	$\bar{\tau}$	Stress tensor [Pa]
σ	Stephen poltzman constant	σ_s	Scattering coefficient
σ_ϵ	The turbulent Prandtl numbers for ϵ	σ_k	The turbulent Prandtl numbers for k
Ω	Spatial solid angle		
Abbreviations			
ACH	Air change per hour	DO	Discrete ordinates
CFD	Computational fluid dynamics	PMV	Prediction mean vote
DR	Draft risk	PPD	Prediction percent of dissatisfaction
Subscripts and superscripts			
ma	mean air	op	oprating

1. INTRODUCTION

The radiant ceiling system uses direct energy transfer from surfaces in the room via modular-style panels to provide a sustainable heating and cooling solution with little air ventilation. The buried copper tubing on the back of the panels is used to circulate hot or cold water. According to estimates [1] and [2], the building

construction industry generates 17% of the world pollution emissions while consuming an estimated 40% of the energy generated globally. The latest report on global energy consumption forecasts addressed several issues with the rise in energy use in modern structures [2]. The rising rates of urbanization are predicted to cause space-cooling/annual energy demand to increase to 260 TWh by 2025. Two alternative solutions are frequently offered to

address this issue. These actions comprise 1) using a cooling system that is more energy-efficient [3] and 2) improving the building envelope for modern construction [4]. The air conditioning systems' typical cooling temperature may rise by 3.0 °C as a result of these actions [2]. Vashistha and Talukdar [5] utilize a unique panel that can react to both sensible and latent load. The goal of this work is to use CFD simulations to examine how the heat and moisture transfer panel (HAMP) performs when it is installed in a room. Nguyen and Reiter [6] utilize CFD to assess how a building's ceiling configuration may affect interior natural ventilation. The major findings show that, although these impacts are rather small, ceiling configurations do have some effects on ventilation flow rates and indoor airflow. Although the radiant ceiling cooling panel (RCCP) system has been demonstrated to be both thermally and economically effective, it is unable to stop specific hot air flows from windows. Ye et al. [7] study combined an innovative, segmented, concave-surface RCCP with a forced ventilation system. The results demonstrate that the ventilation system is successful in stopping the hot air flow and that it greatly enhanced the cooling effectiveness of the RCCP. Using a hybrid numerical optimization approach, a heating hydronic radiant panel system for the walls and ceiling of a typical residential structure was investigated. The methodology and results are presented in the hybrid numerical optimization study. The location, size, and temperature of the fluid inflow are the primary design parameters. Results reveal that a family of optimum designs rather than a single optimal solution exists [8]. Newly developed terminal device experiments and computational approaches were utilized to study the exposed capillary ceiling radiant panels (E-CCRP) system, which is becoming more and more common in public buildings. Thermal radiation and natural convection work together to transfer heat between the system and the interior environment. The system must be operated in real-time, and the radiation system latent heat transfer latency must be taken into account [9]. A decoupled radiant cooling unit (DRCU) can boost cooling capacity while lowering the danger of condensation. The current study created a computational fluid dynamic model for the purpose of investigating the temperature environment within a tiny chamber. Investigations were conducted on four examples with different radiant cooling temperatures and different radiant cooling areas. The findings showed that the low radiant cooling temperatures produced by the DRCU thermal comfort and thermal environment met the requirements of the ASHRAE Standard for comfort [10]. By using numerical simulations in a radiant heating room with a diffuse ceiling ventilation system and varied porous ceiling opening rates, the flow field distribution was examined. The findings showed that irregular openings in the porous ceiling might improve the interior asymmetric thermal environment and reduce uncomfortable local draughts under various porous ceiling opening rates. The way in which fresh air was introduced toward the radiant heating room made a difference in the asymmetric thermal

environment [11]. In evaluating the inside thermal environment, further particular considerations must be taken into account given the differences in internal heat transmission processes compared to frequently utilized air systems. For instance:

- 1- Due to the reduced surface temperature, the air draught rate might be a significant problem. Moreover, the decreased ventilation rates, or semi-stagnant interior air, may make inhabitants feel uneasy.
- 2- The possibility of thermal discomfort is increased by the thermal activation of specific enclosure surfaces due to radiation asymmetries.
- 3- To assess the risk of water vapor condensation, the dew point temperature variation must be evaluated.
- 4- When the ground is the active surface, the vertical temperature differential is a significant issue.

The thermal performance and energy consumption of a radiant ceiling heating system that serves four distinct room types within the same building are investigated [12]. The findings indicate that the intensity of the energy use for heating is around 19.63 W/m², which is roughly 30% less than the heating index recommended in the regional standard. The interior temperature conditions of the various sorts of rooms differ from one another as well. The amount of occupied space, exterior cold air penetration, and solar radiation are the main factors influencing the interior thermal climate. Using radiant ceiling heating in bigger spaces consumes less energy since the internal temperature conditions are frequently better. In light of this, systems that use radiant ceiling heating are more suited for bigger spaces. Temperatures within and outside the room were measured experimentally. A numerical simulation was also employed to analyze the room flow pattern and anticipate the temperature distribution. The model was employed to investigate the effects of panel heater placement and size on airflow and temperature distribution. The full-size room could be replicated by the scale room model with a negligible error of 20% or less, particularly in terms of heater load, and the temperature distribution was close to 1%. It was found that using the heating panel on the floor resulted in the lowest heat transmission rates [13]. In a scaled-down experiment, a combined system that combines diffuse air flow with a radiant ceiling panel was examined. The perforated radiant ceiling panel rate-dependent heat transfer was to be mapped as part of the experiment. The heat transfer coefficient for cooling cases improved by 20% from no ventilation to a high ventilation rate, and the findings were most accurate for the moderate values (14 W/m²) of these values. A high radiative-to-convective ratio was found to be a result of the room internal heat gain. The heating scenarios failed to demonstrate a definite shift [14]. According to [15–17], no research paper has previously studied the effect of a transparent ceiling with hidden radiative ceiling cooling in any previous study.

2. METHODOLOGY

2.1 GEOMETRY DESCRIPTION

The main room dimensions are (4 × 3 × 2.5 “length × width × height”) m, the dimensions of the hidden part of the room above the transparent ceiling (acrylic ceiling) are (4 × 3 × 0.5 “length × width × height”) m, the air supply grille on the wall of hidden part of the room has a

dimensions of (2 × 0.1 “width × height”) m, the air return grille on the wall of main room has a dimensions of (0.6 × 0.2 “width × height”) m, the air entry hole on the acrylic ceiling in the middle of ceiling with a dimensions of (0.3 × 0.3 “width × height”) m, and the two lighting sources with dimensions of (1.2 × 0.1 “width × height”) m. Finally, a LED screen computer with dimensions of (0.2 × 0.6 “width × height”) m is positioned as displayed in Figure 1.

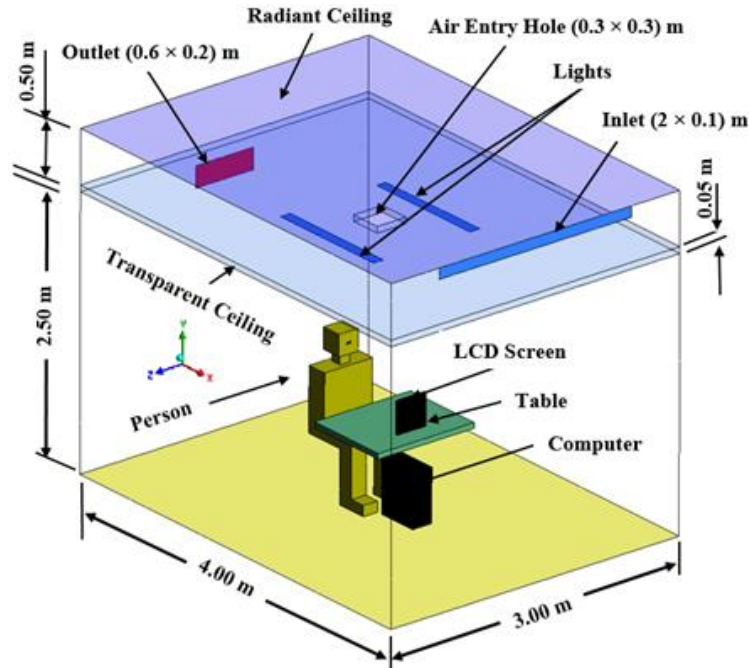


Figure 1 An isometric perspective of the problem computational domain

2.2 GOVERNING EQUATIONS

A compressible fluid 3D internal turbulent flow can be thought of as the present issue. The viscous losses are taken into consideration while the system is investigated under steady-state operating settings. Therefore, the following equations (Eqs. (1)– (4)) for the air control volume needs to be solved for steady-state conservation of mass, momentum, and energy[18]:

$$\nabla \cdot (\rho \vec{v}) = 0 \tag{1}$$

$$\nabla \cdot \rho \vec{v} \vec{v} = -\nabla P + \nabla \cdot (\overline{\tau}) + \rho \vec{g} \tag{2}$$

$$\nabla \cdot (\vec{v}(\rho E + P)) = \nabla \cdot (\rho k_{\text{eff}} \nabla T - \vec{h} + (\overline{\tau}_{\text{eff}} \cdot \vec{v})) \tag{3}$$

$$E = h - \frac{P}{\rho} + \frac{v^2}{2} \tag{4}$$

DO Radiation model, [9]

$$\begin{aligned} \nabla \cdot (I(\vec{r}, \vec{s}) \vec{s}) + (a + \sigma_s) I(\vec{r}, \vec{s}) & \tag{5} \\ = an^2 \frac{\sigma T^4}{\pi} & \\ + \frac{\sigma_s}{4\pi} \int_0^{4\pi} I(\vec{r}, \vec{s}) \phi(\vec{r}, \vec{s}) d\Omega & \end{aligned}$$

For H₂O, distribution of species concentrations was also investigated eq. (6).

$$\nabla \cdot (\rho \vec{v} Y_i) = -\nabla \cdot \vec{J}_i + S_i \tag{6}$$

$$\vec{J}_i = -\rho D_{i,m} \nabla Y_i - D_{T,i} \frac{\nabla T}{T} \tag{7}$$

The two-equation (k-ε) turbulence model, which predicts the turbulence viscosity based on the turbulence kinetic energy (k) and how it rate of (ε) dissipates, is used to account for the turbulence effect. According to [19], the Prandtl-Kolmogorov equation indicates that the turbulent viscosity in this model is related to the turbulence kinetic energy (k) and dissipation rate (ε), respectively.

$$\frac{\partial}{\partial x_i}(\rho k u_i) = \frac{\partial}{\partial x_j} \left[\left(\mu + \frac{\mu_t}{\sigma_k} \right) \frac{\partial k}{\partial x_j} \right] + G_k + G_b - \rho \varepsilon - Y_M + S_k \quad (8)$$

and

$$\frac{\partial}{\partial x_i}(\rho \varepsilon u_i) = \frac{\partial}{\partial x_j} \left[\left(\mu + \frac{\mu_t}{\sigma_\varepsilon} \right) \frac{\partial \varepsilon}{\partial x_j} \right] + G_{1\varepsilon} \frac{\varepsilon}{k} (G_k + C_{3\varepsilon} G_b) - C_{2\varepsilon} \rho \frac{\varepsilon^2}{k} + S_\varepsilon \quad (9)$$

$$\mu_t = \frac{C_\mu \rho k^2}{\varepsilon}, \text{ where } C_\mu = 0.09 \quad (10)$$

This section provides the definitions of overall thermal comfort that are used to evaluate the thermal environment inside the office room. The prediction mean vote (PMV), prediction percent of dissatisfaction (PPD). PMV measures the thermal sensitivity of the human body to hot and cold on a scale from +3.0 (very hot) to -3.0 (very cold). When PMV gets close to zero, people inside tend to feel more comfortable. To accommodate different settings, [20-23] updated the Fanger model, a well-known measure of thermal comfort. Their model is stated as follows:

$$PMV = 0.09982 \times \left\{ 40 - \frac{1}{B} \left[\left(34.6 - \frac{4.7T_r + h_c T_{ma}}{4.7 + h_c} \right) + 0.37623 \times (5.52 - P_v) \right] \right\} - 0.09979 \times [0.0562 \times (34 - T_{ma}) + 0.692 \times (5.87 - P_v)] \quad (10)$$

$$h_c = \begin{cases} 5.1 \left[\frac{W}{m^2} \cdot K \right] & \text{for } 0.00 < v < 0.15 \frac{m}{s} \\ 2.7 + 8.7 v^{0.669} \left[\frac{W}{m^2} \cdot K \right] & \text{for } 0.15 < v < 1.50 \frac{m}{s} \end{cases} \quad (11)$$

Since of a predetermined clothing factor of 0.5 clo, the thermal resistance of the seating arrangement (B) is assumed 0.261655 m².K/W. The percentage of unsatisfied occupants subjected to the same heat environment is quantified by PPD [20-23]. It is directly connected to PMV in the way as follows:

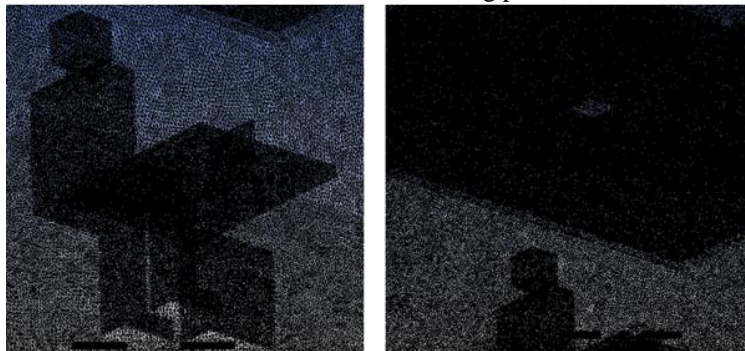


FIGURE 2. Mesh generation view at person and radiant ceiling (more than 6,700,000 cells)

$$PPD = 100.0 - 95.0 \times \exp(-0.03352 \times PMV^4 - 0.21792 \times PMV^2) \quad (12)$$

[-0.5] ≤ PMV ≤ [0.5] satisfied range] is the recommended range under ISO 7730 [21].

A local thermal disturbancesigns must be assessed in radiant cooling situations. This contains the minimum surface temperature, relative humidity (RH), local air temperatures, and local air velocity, draft risk. An occupant thermal perception of air flow around their body is measured by the Draft Risk (DR). As defined in this context, DR [21]

$$DR = (34 - T_{ma}) \times (v - 0.05)^{0.6223} \times (0.37 * TI + 3.143) \quad (13)$$

The minimum radiating surface temperature can be compared to the greatest local dew point temperature to establish condensation risk (CR). The temperature at which the equal amount of heat exchanged among the radiating surface and the non-uniform actual temperature surface is known as the operating temperature (Top). Top was established as [21]:

$$T_{op} = \frac{h_r T_r + h_c T_c}{h_r + h_c} \quad (14)$$

2.3 GRID GENERATION

The surface model was created with ANSYS design-modeler. The surface geometry generated by the design-modeler tool was used to create an accurate mesh in the form of an MSH file. The mesh file was uploaded to FLUENT along with the necessary flow boundary conditions and the flow equations needed to be solved. The mesh dependency was examined by resolving the flow domain of five mesh structures with 879,500, 1,476,000, 2,200,000, 3,670,000, and 6,730,000 elements, respectively, as show in Figure 2. The findings revealed that the two finer and coarser meshes differed by 0.5% and 6.45%, respectively. The mesh gradually enlarges until it reaches 0.05 m in the remaining portion of the room, where it is particularly dense adjacent to the ceiling cooling panel.

2.4 VALIDATION OF THE MODEL

A comparison was done to evaluate the validity and applicability of the current CFD model. Figure 3 and 4 show a comparison of the observed results with observed results [6, 7] using the widely used k-ε turbulence model. The findings show that there are variations at some sites as well as in some areas of the planes where the measured and simulated values are the same. However, the numerical figures follow the same trend and fall within an acceptable range of temperature and velocity. The outcomes demonstrated that the numerical approach utilized could correctly forecast the velocity distribution in the room.

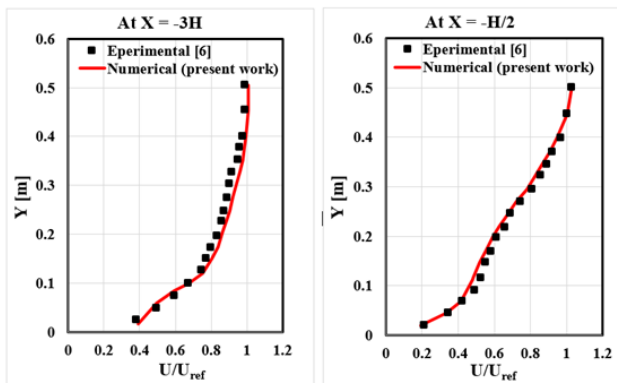


FIGURE 3. Comparison of the experimental and numerical results [6]

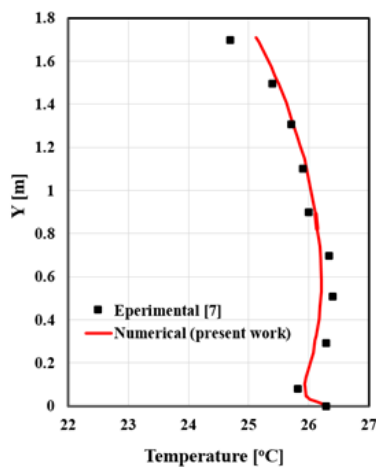


FIGURE 4. The validation of the CFD model with experimental result in the middle line [7]

2.5 NUMERICAL SOLUTION STABILITY

Before the simulation begins, two critical recurrence parameters must be set: the relaxation factor, which governs the resolution of the solution for each iteration, and the segment remaining value, which controls when the repeat process can be terminated. Relaxation factors were utilized to boost the solution stability because of the significant number of fluctuations in the solution. Under Near-Wall Treatment, choose Enhanced Wall Treatment, and under Options, choose Full Buoyancy Effects. The velocity and pressure flow fields were connected using the

SIMPLE approach. Iterations were stopped when the energy equation relative error was less than 10^{-7} and 10^{-4} for the other solved equations. Internal radiative heat transfer has also been treated using the discrete ordinate (DO) model. The DO model was chosen for the radiation model since it can be applied with excellent accuracy in the majority of scenarios and numerous considerations were taken into consideration.

It was assumed that the expelled gases of the passengers during respiration, which had a temperature of 37 °C and a speed of 0.3 m/s, consisted of nitrogen, carbon dioxide, and water vapor. The ratios of H₂O and CO₂ ejected gases were 0.043 and 0.05 as mass units, respectively [24]. The dimensions of the nose were (0.05 m × 0.02 m).

2.6 BOUNDARY CONDITIONS

Wall heat fluxes have been described as not present in visible or invisible room walls, furniture, or other non-heat dissipating components. The room under study has an air change per hour (ACH) of 2 and 3, which is recommended by ASHRAE [25], and an inlet air supply temperature (T_a) of 19, 21, 23, and 25 °C, an inlet relative humidity of 50%, and an inlet CO₂ of 500 ppm. Also, the mean radiant ceiling temperature (T_p) where four values of 19, 21, 23, and 25 °C with an emissivity of 0.7. The heat source values in the office room are shown in Table 1.

TABLE 1. Boundary conditions of the office room

Heat Source Name	Heat Flux W/m ²	Emissivity, ε	Amount t
Fluorescent lamp	32.5 [23]	0.9	2
LCD screen	36 [23]	1	1
Human body	60 [25]	0.9	1
Computer	82 [25]	1	1
Floor	Adiabatic, [26]	0.3	1
Walls	Adiabatic, [26]	0.07	8

3. RESULTS AND DISCUSSIONS

The thermal setting of an office room is covered in the first portion of this article in terms of general thermal comfort measures (section 3.1). Next, it is determined if the radiant ceiling panel could experience water vapor condensation (section 3.2), Carbon Dioxide level (section 3.3), and cooling capacity (section 3.3). Finally, the effect of computer heat dissipation is examined (section 3.4). Case code, for example, has the number (25253), the first two numbers are the cooling panel temperature; the second two numbers are the supply air temperature to the room; and the final number is the ACH.

3.1 OVERALL THERMAL COMFORT

Figure 5 displays scatter graphs of PPD against PMV that represent the general human thermal sensitivity in all scenarios under investigation. ISO standard 7730 [27] and In ASHRAE standard 55 [21], the three permissible thermal comfort levels are specified. Both standards define the three groups A, B, and C as having ranges of [0, 6], [6, 10], and [10, 15] for PPD and [-0.2, 0.2], [-0.5, 0.5], and [-0.7, 0.7] for PMV. Group A denotes the greatest quality of internal environments. Figure 3 shows the range of operating options available for preserving various degrees of thermal comfort despite the somewhat high supply air and panel surface temperatures that were taken into consideration. The 32 studied scenarios, 16 have 2 ACH and the remaining 16 have 3 ACH, are divided into 5 groups A, 8 groups B, 4 groups C, and 15 instances that fall outside of what is acceptable in occupied regions. The cases that belong to grade A are (25192, 25252, 23252, 25233, and 23253); their PMV values range from 0.18 to 0.13 and their PPD values from 5.08 to 5.3%. Among the 15 instances of unsuitable circumstances inside. However, case selection (23252) does save air at 25 °C, which is advantageous because cooling water uses less energy than cooling air (water has a higher specific heat capacity and density than air). In this case, low-quality thermal systems such as geothermal or solar sources can be used to condition both the water and air supply.

Figure 6 shows scatter graphs of average radiant temperature (Tr) against average air temperature (Tma) for 32 studied cases. When each of the three tuned components (Tam, Tp, and ACH) increases while the other factors stay the same, the semi-linear correlations between (Tr) and (Tma) are displayed in Figure 5. As expected, both the panel temperature and the incoming air temperature

increase with each ACH number. But both temperatures only slightly decrease when the panel ACH decreases. The {Tr, Tam} values for instances (2325) ACH are {25.05, 26.18} and {25.01, 25.69} oC, respectively, for e values of 2 and 3 ACH. The mean temperature of the air volume will decline when the temperatures of all non-radiant surfaces decrease as a result of an increase in the convective heat transfer rate from the hotter source.

Additionally, Figure 6 shows that comfortable levels may be attained at quite high mean air temperatures, up to 27.32 oC (case 25252). The comparatively low mean radiant temperatures, as low as 23.6 oC, offset these higher air temperature levels (case 23192). The operative temperatures, which are likewise shown in Figure 7, indicate the combined influence of the two temperatures. Additionally, this graph demonstrates that Top grows significantly with the Tr but less so with Top. The modest variations in operating temperature (Top) for the identical panel and air temperatures but considerable variations in ACH are related to the various radiative heat transfer coefficients that are linked with them.

3.2 CONDENSATION RISK

When the panel surface temperature is higher than the dew point temperature, water vapor condensation occurs. With reference to Figure 5, example 19193, when the dew point temperature is just 13.73 oC, has the lowest Tma = (20.95 oC). This temperature differential is far more than the minimal safety margin often advised (1.0-1.5 oC) for preventing condensation problems. Additionally, there is a 7.22 oC temperature difference between the dew point temperature for each case and the lowest local air temperature under all scenarios (19 oC for case 23192). (5.27 oC). Thus, it can be said that there is no need for concern regarding condensation dangers.

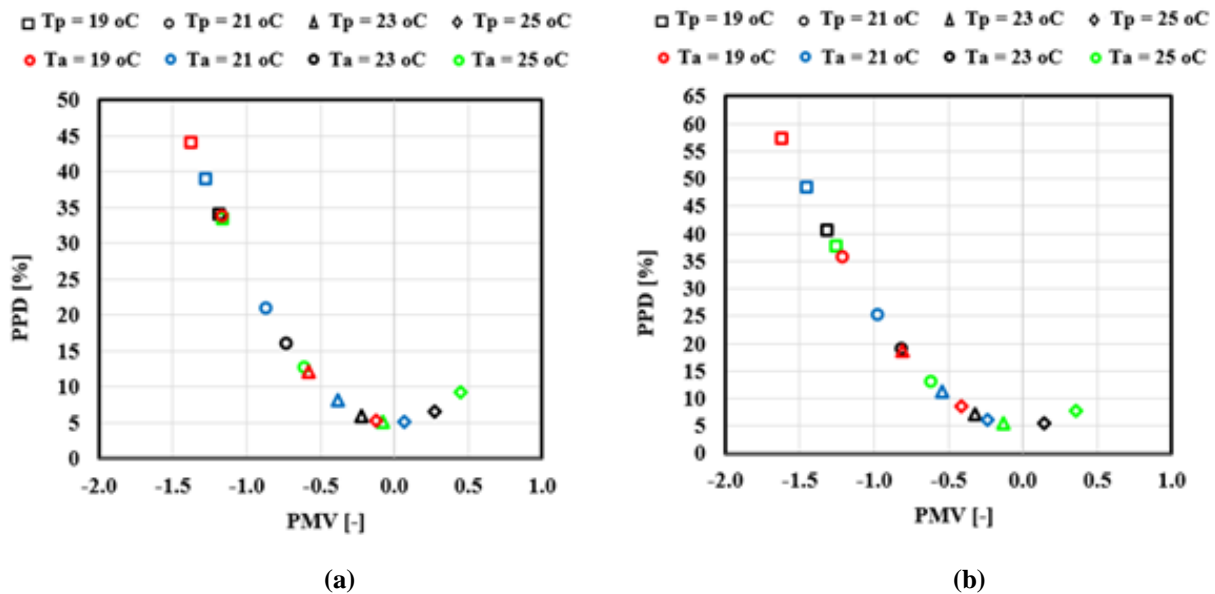


FIGURE5. PPD versus PMV scatter graphs for 32 simulated scenarios. Ta and Tp values are shown by the kind and color of the marking, respectively. (a) At 2 ACH and (b) At 3 ACH

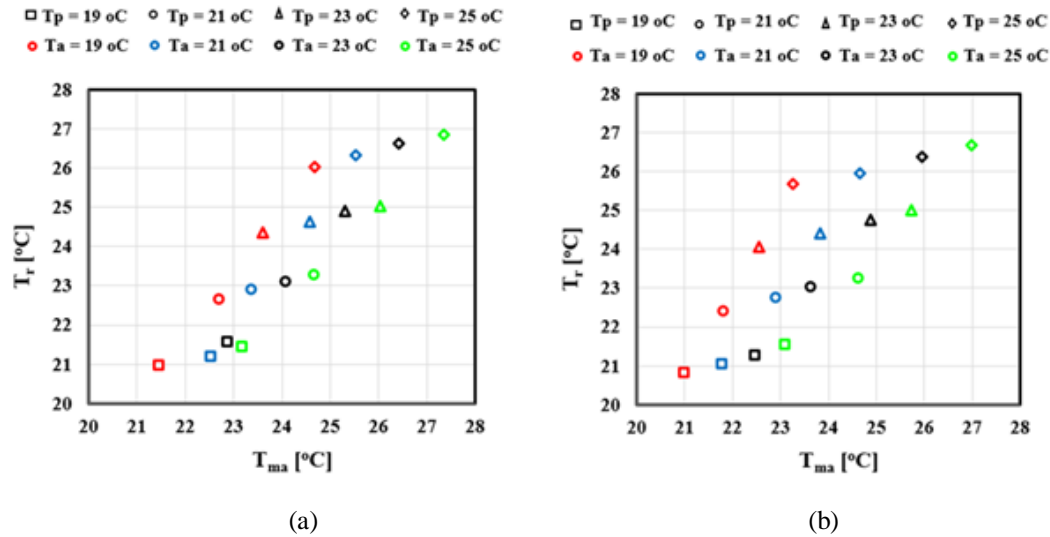


FIGURE6.Scatter graphs of average radiant temperature (T_r) against average air temperature (T_{ma}) for 32 simulated cases. (a) At 2 ACH and (b) At 3 ACH

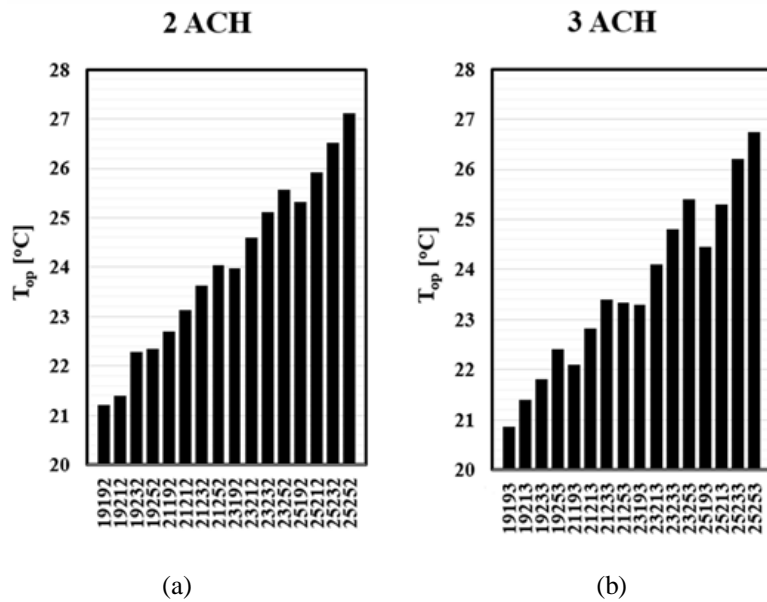


FIGURE7.Bar graphs of operative temperatures for 32 studied cases

3.3 CARBON DIOXIDE LEVEL

All cases have a CO2 level below the CO2 value recommended by the ASHRAE standard of 1,000 ppm. When studying the proportion of carbon dioxide in the room, it was found that it was far from the level of 1000 ppm.

3.4 COOLING CAPACITY

Figure 8 shows radiative and convective heat of cooling capacities (CCs) of the radiant ceiling panel for 32 studied cases. In order to examine the radiative portion of the overall cooling capacity, the entire heat flow on the panel surface is divided into radiative and convective cooling capabilities. Radiant systems are often defined as having a radiative heat transfer contribution of 50% or

more. This was achieved in some cases, and others were not. However, just five cases did so, as seen in Figure 6, despite the fact that the proportion is 19.16-60.1%. The reason is that in the present estimations of CC, both convective and latent loads (fresh air supply and occupant) are taken into account. As T_p falls and/or ACH rises, the total CC rises, as would be predicted by the fundamental radiation equation of Boltzmann. The overall CC rises when T_a rises. This is explained by the fact that, due to noticeably hotter air streams, the average temperatures of non-activated walls have risen, which resembles the increases that have been seen in cooling capacity brought on by higher enclosure temperatures. The range of total cooling capacity is 6.1 (case 21193) to 25.08 (case 19252) W/m².

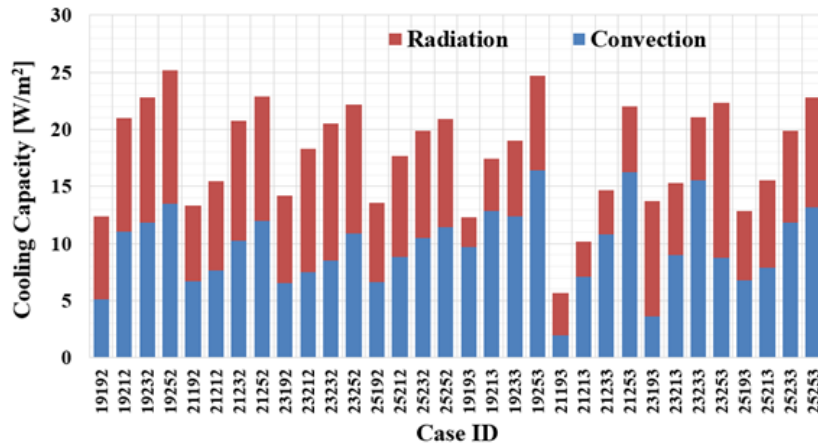


FIGURE8.Convective and radiative heat cooling capacities of the radiant panel for 32 simulated cases

3.5 IMPACT OF HEAT DISSIPATION

Since computers normally work for brief periods of time, the heat dissipation rates from such devices have thus far been disregarded. Given the dissipation rates listed in Section 2.6, another simulation based on example (23252) has been run. Figure 8 shows the boundaries of the occupancy local temperature and draught danger as well as the walls and lighting of the office room. With an increase in heating demand, the room temperature rises noticeably. But the operating temperature is still within acceptable ranges (of 24.9 oC). However, the new PMV

value (0.31) indicates a little warming (at the beginning of group B). The dew point temperature rises marginally to 16.83 oC, which is 4.17 oC lower than T_p , as a result of an increase in T_{ma} . This means that no condensation will occur inside the office room. The decreasing draft risk (by 11.44%) is also a result of the increased T_{am} since the occupant sensitivity to cold air streams lowers. Because radiative and convective losses from the computer are directly absorbed, the CC of the panel improves by 6.65%, with a greater percentage of radiative heat transfer of 15.47%.

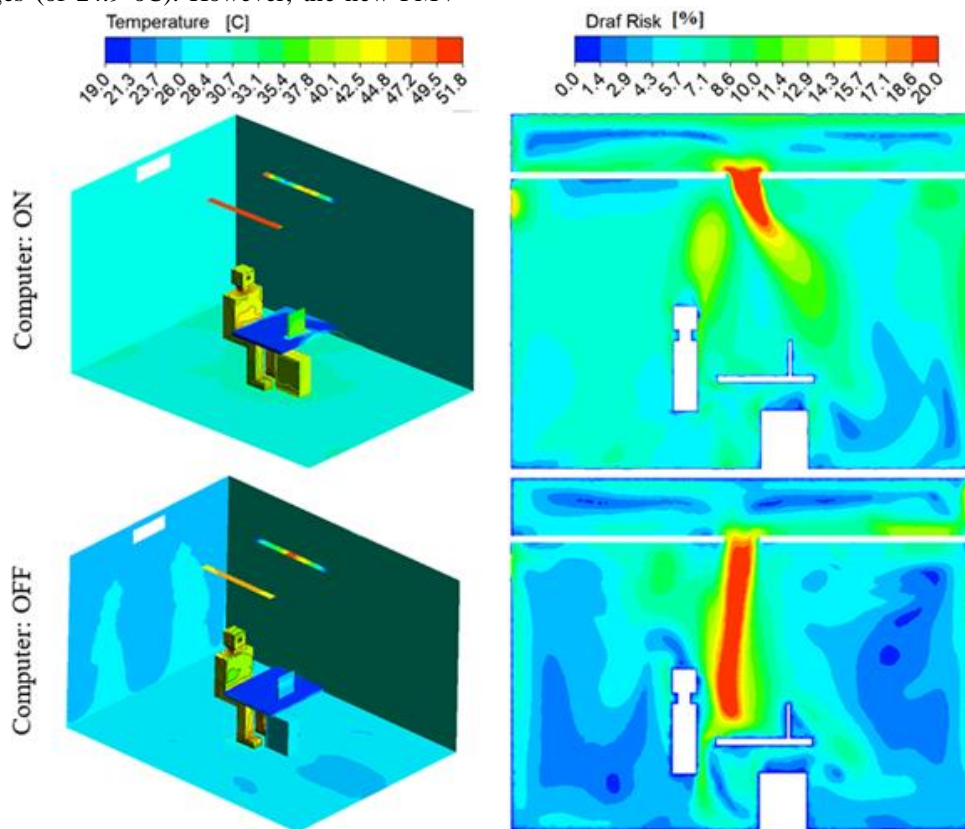


FIGURE9.Contours of temperature distribution and draft risk when the computer is switched ON and OFF ($T_r = 21$ °C, $T_a = 25$ °C, and ACH = 2)

4. CONCLUSIONS

This study examines the RCCP system cooling capacity and interior thermal comfort when paired with forced ventilation. The transparent surface prevents any possibility of water leakage, which could condense as a result of the cooling panel if it occurred without affecting the heat exchange by radiation. It also works to mix the incoming air after the radiation heat exchange with the different surfaces inside the room. The ceiling panel is used to regulate the temperature and relative humidity inside the office room to achieve good thermal comfort and energy savings. The results indicate that the CFD model was in good agreement with the experimental results, with an average error rate of 3.2% and 4 % for air velocity and temperature, respectively.

Additionally, the ventilation flow rates have less of an effect than the ventilation inlet temperature, which is followed by the panel surface temperature. This means that the number of ACH can be less than 2, according to this study, which relied on ASHRAE for this value (from 2 to 3 ACH, [24]) to give good indoor air quality. The optimal ventilation air temperature and air change per hour are 25 °C and 2, respectively, while a panel surface temperature of 21 °C increases thermal comfort while lowering energy consumption. Additionally, there are no concerns of condensation. The range of total cooling capacity is 6.1 (case 21193) to 25.08 (case 19252) W/m². All cases have a CO₂ level below the CO₂ value recommended by the ASHRAE standard of 1,000 ppm.

REFERENCES

- [1] L. Belussi, B. Barozzi, A. Bellazzi, L. Danza, A. Devitofrancesco, C. Fanciulli, M. Ghellere, G. Guazzi, I. Meroni, F. Salamone, F. Scamoni, C. Scrosati, A review of performance of zero energy buildings and energy efficiency solutions, *J. Building Engineering*, volume 25, (2019), pages 100772.
- [2] International Energy Agency, World Energy Outlook 2020: Part of World Energy Outlook, World Energy Outlook 2020, IEA, Paris. 2050; 2020:1–25. <<https://www.iea.org/reports/world-energy-outlook-2020>>.
- [3] Z. Li, D. Zhang, X. Chen, C. Li, A comparative study on energy saving and economic efficiency of different cooling terminals based on exergy analysis, *J. Building Engineering*, Volume 30, (2020), Pages 101224.
- [4] [4] Z. Liu, L. Zhang, G. Gong, T. Han, Experimental evaluation of an active solar thermoelectric radiant wall system, *Energy Conversion Management*, Volume 94, (2015), Pages 253–260.
- [5] V. Vashistha, P. Talukdar, Numerical studies for performance evaluation of a permeable ceiling panel for regulation, *Energy and Buildings*, Volume 62, (2013), Pages 158–165.
- [6] A. Tuan Nguyen, S. Reiter, The effect of ceiling configurations on indoor air motion and ventilation flow rates, *Building and Environment*, Volume 46, (2011), Pages 1211–1222.
- [7] Minzhi Ye, Ahmed A. Serageldin, Katsunori Nagano, CFD simulation on the thermal performance of a novel radiant ceiling cooling panel (RCCP) system with segmented and concave surface a combined with forced ventilation, *Energy Reports*, Volume 6 (2020) 1519–1524.
- [8] M. Tye-Gingras, L. Gosselin, Comfort and energy consumption of hydronic heating radiant ceilings and walls based on CFD analysis, *Building and Environment*, Volume 54, (2012), Pages 1-13.
- [9] Z. Jing, L. Jiayu, Study on heat transfer delay of exposed capillary ceiling radiant panels (E-CCRP) system based on CFD method, *Building and Environment*, Volume 180, (2020), Pages 106982.
- [10] Yuying Liang, Nan Zhang, Huijun Wu, Xinhua Xu, Ke Du, Jianming Yang, Kaijun Dong, Gongsheng Huang, Qin Sun, Thermal environment and thermal comfort built by decoupled radiant cooling units with low radiant cooling temperature, *Building and Environment*, Volume 206, (2021), Pages 108342.
- [11] Bin Yang, Yuyao Guo, Shuaixing Xu, Wei Su, Mengchun Wu, Faming Wang, Performance optimization of a sidewall radiant heating system integrated with diffuse ceiling ventilation, *Building and Environment*, Volume 213, (2022), Pages 108881.
- [12] Wei Liao, Yimo Luo, Jinqing Peng, Dengjia Wang, Chenzhang Yuan, Rongxin Yin, Nianping Li, Experimental study on energy consumption and thermal environment of radiant ceiling heating system for different types of rooms, *Energy*, Volume 244, (2022), Pages 122555.
- [13] Shaimaa Seyam, Ahmed Huzayyin, Hesham El-Batsh, Sameh Nada, Experimental and numerical investigation of the radiant panel heating system using scale room model, *Energy and Buildings*, Volume 82, (2014), Pages 130–141.
- [14] Marie Rugholm Krusaa, Christian Anker Hviid, Reduced-scale experiments of heat transfer from integrated radiant ceiling panel and diffuse ceiling ventilation, *Applied Thermal Engineering*, Volume 197, (2021), Pages 117348.
- [15] Kyu-Nam Rhee, Kwang Woo Kim, A 50 year review of basic and applied research in radiant heating and cooling systems for the built environment, *Building and Environment*, Volume 91, (2015), Pages 166-190.
- [16] Esmail M. Saber, Kwok Wai Tham, Hansjürg Leibundgut, A review of high temperature cooling systems in tropical buildings, *Building and Environment*, Volume 96, (2016), Pages 237-249.
- [17] [17] Fan Zhang, Heinz-Axel Guo, Zhengxuan Liu, Guoqiang Zhang, A critical review of the research about radiant cooling systems in China, *Energy & Buildings*, Volume 235, (2021), Pages 110756.
- [18] J.D. Anderson, *Governing equations of fluid dynamics*, Computation Fluid Dynamics, (2009), Pages 15-51.
- [19] A. E. A. E. Degwy, S. M. Morkos, A. S. Sabry, and E. E. Khalil, Numerical computations of flow regimes in enclosed spaces, *Proceedings ASME Des. Eng. Tech. Conf.*, Volume 5, (2012), Issue 2, Pages 817–824.
- [20] [20] Z. Lin and S. Deng, “A study on the thermal comfort in sleeping environments in the subtropics-Developing a thermal comfort model for sleeping environments,” *Build. Environ.* vol. 43, no. 1, pp. 70–81, 2008.
- [21] O. A. Ismail, M. A. Kassem, M. A. Hassan, sleeping pods with radiant cooling panels: A first assessment of thermal comfort and cooling capacity, *Energy & Buildings*, Volume 250, (2021), Pages 111282.
- [22] A. Eldegwy and E. E. Khalil, Passengers’ thermal comfort in private car cabin in hot climate, *Joint Propulsion Conference*, (2018), Pages 1–11.
- [23] ASHRAE Standard 55, Thermal Environmental Conditions for Human Occupancy, ASHRAE Inc., Atlanta USA, 2017.
- [24] “American Society of Heating, Refrigeration, and Air-Conditioning Engineers, ANSI/ASHRAE 62: ventilation for Acceptable Indoor Air Quality, Atlanta, GA, ASHRAE, 2019.
- [25] J. Du, M. Chan, D. Pan, S. Deng, A numerical study on the effects of design/operating parameters of the radiant panel in a radiation-based task air conditioning system on indoor thermal comfort and energy saving for a sleeping environment, *Energy Building*, Volume 151, (2017), Pages 250–262.
- [26] “R. and A.-C.E. (ASHRAE) The American Society of Heating, Thermal environmental conditions for human occupancy, Atlanta, GA; 2013.
- [27] ISO, ISO 7730: Ergonomics of the thermal environment Analytical determination and interpretation of thermal comfort using calculation of the PMV and PPD indices and local thermal comfort criteria; 2005.